Journal of Alloys and Compounds 506 (2010) 57–62

Contents lists available at ScienceDirect

Journal of Alloys and Compounds

journal homepage: www.elsevier.com/locate/jallcom

RuO_2–SnO_2 nanocomposite electrodes for methanol electrooxidation

Jong-Min Lee, Sang-Beom Han, Young-Woo Lee, You-Jung Song, Jy-Yeon Kim, Kyung-Won Park*

Department of Chemical and Environmental Engineering, Soongsil University, Seoul 156-743, South Korea

ARTICLE INFO

Article history:
Received 18 February 2010
Received in revised form 23 June 2010
Accepted 6 July 2010
Available online 14 July 2010

Keywords:
Ruthenium-tin oxides
Nanocomposite
Support
Colloidal method
Methanol electrooxidation

ABSTRACT

The RuO_2–SnO_2 nanostructured electrodes for methanol electrooxidation are prepared by means of colloidal synthetic method. Using X-ray diffraction method and transmission electron microscopy, it is observed that the crystallinity of nanocomposite supports is increased with heat treatment due to an increased crystallinity of SnO_2 and RuO_2 nanophases with ~5 nm in size. In the case of the $RuSnO_2$ supported catalysts, Pt nanocatalysts with ~3 nm in size are well dispersed and mixed with $RuSnO_2$ nanocomposite supports. Using an electrochemical and thermogravimetric analysis, it is found that the $RuSnO_2$ supported catalysts show an excellent catalytic activity and stability in comparison with Vulcan XC-72 supported catalyst. Furthermore, compared to the Pt catalyst supported by as-prepared $RuSnO_2$, the Pt catalyst supported by $RuSnO_2$ heated at 400 °C displays an excellent catalytic activity and stability, which could be due to an increased crystallinity caused by heat treatment.

1. Introduction

Direct methanol fuel cells (DMFCs) have attracted considerable interest because of a variety of merits such as low operating temperatures, ease of handling a liquid fuel, the high energy density of methanol, and applications to micro-sized fuel cells [1,2]. The excellent catalytic activity of platinum for methanol oxidation, especially, at low temperatures makes this metal electrocatalyst ideal for use as an anode in DMFCs. However, to confirm an excellent performance and stability of the fuel cell, such an electrode consists of a metallic nanophase and a porous material as a support for the nanoparticles.

Typically, carbon-based nanomaterials have been used as promising supports for low temperature fuel cells. Carbon black has been well known as an ideal material for supporting nanosized metallic particles in the electrode for polymer electrolyte membrane fuel cells. However, kinetically slow, yet thermodynamically favourable electrochemical oxidation of carbon at fuel cell potentials limits long-term stability of the supported catalysts [3–14]. Despite the relatively low operation temperature in the fuel cell, the electrode encounters conditions favourable to oxidation such as the presence of oxygen, liquid water, and high potentials. Accordingly, carbon substitutes are extremely needed for much longer life time in fuel cell operation.

In general, the requirements of support materials for their applications to the supports for platinum-based electrocatalyst are a high surface area for well-dispersion of nanosized catalysts, low electrical resistance to facilitate electron transport during the electrochemical reactions, a pore structure suitable for maximum contact with fuel or oxidant and strong interaction between the catalyst and the support. Especially, oxide supports have been widely used in heterogeneous catalysis and have inherently higher stability than carbon in oxidizing environments. Among them, tin oxides have been attractive as supports due to stability in fuel cell operation atmosphere, low cost, commercial availability, and stability in water. The stoichiometric SnO_2 is a semiconductor with a band gap of 3.0–3.2 eV at room temperature [15–19]. However,

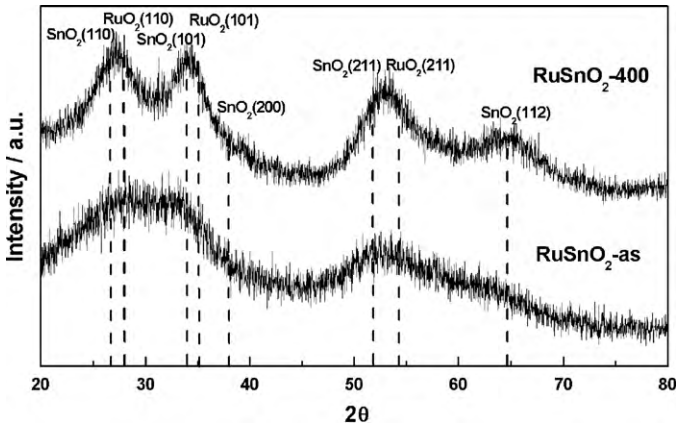

Fig. 1. XRD patterns for as-synthesized RuO_2–SnO_2 ($RuSnO_2$-as) and RuO_2–SnO_2 annealed at 400 °C ($RuSnO_2$-400).

* Corresponding author. Tel.: +82 2 820 0613; fax: +82 2 812 5378.
E-mail address: kwpark@ssu.ac.kr (K.-W. Park).

0925-8388/$ – see front matter © 2010 Elsevier B.V. All rights reserved.
doi:10.1016/j.jallcom.2010.07.012

for electrochemical applications such as DMFC, an excellent electronic conductivity of SnO_2 is necessarily required. The methods to improve an electronic conductivity of SnO_2 are reduction of pure tin oxide by introducing appropriate dopants (F or Sb) and conducting materials (polymer or oxide) in the oxide [20–24].

In this paper, we prepared RuO_2–SnO_2 nanocomposite electrode as a support for DMFCs and evaluated electrochemical properties of RuO_2–SnO_2 supported Pt catalysts compared to those of conventional carbon supported Pt catalyst. The structural and electrochemical properties of the supported catalysts were characterized using transmission electron microscopy (TEM), energy dispersive X-ray spectroscopy (EDX) X-ray diffraction (XRD), voltammetry, and thermogravimetric analysis (TGA).

2. Materials and methods

The RuO_2–SnO_2 nanocomposite electrode with an atomic ratio of Sn:Ru = 50:50 was prepared by colloidal synthetic method [25]. $SnCl_4{\cdot}5H_2O$ and $RuCl_3{\cdot}3H_2O$ were used as precursors. The $SnCl_4{\cdot}5H_2O$ (1.13 g, Aldrich) and $RuCl_3{\cdot}3H_2O$ (0.916 g, Aldrich) were completely dissolved in de-ionized water at 25 °C, and then $NaHSO_3$ (4 g, Aldrich) was added to the precursor solution with continuous stirring for 1 h.

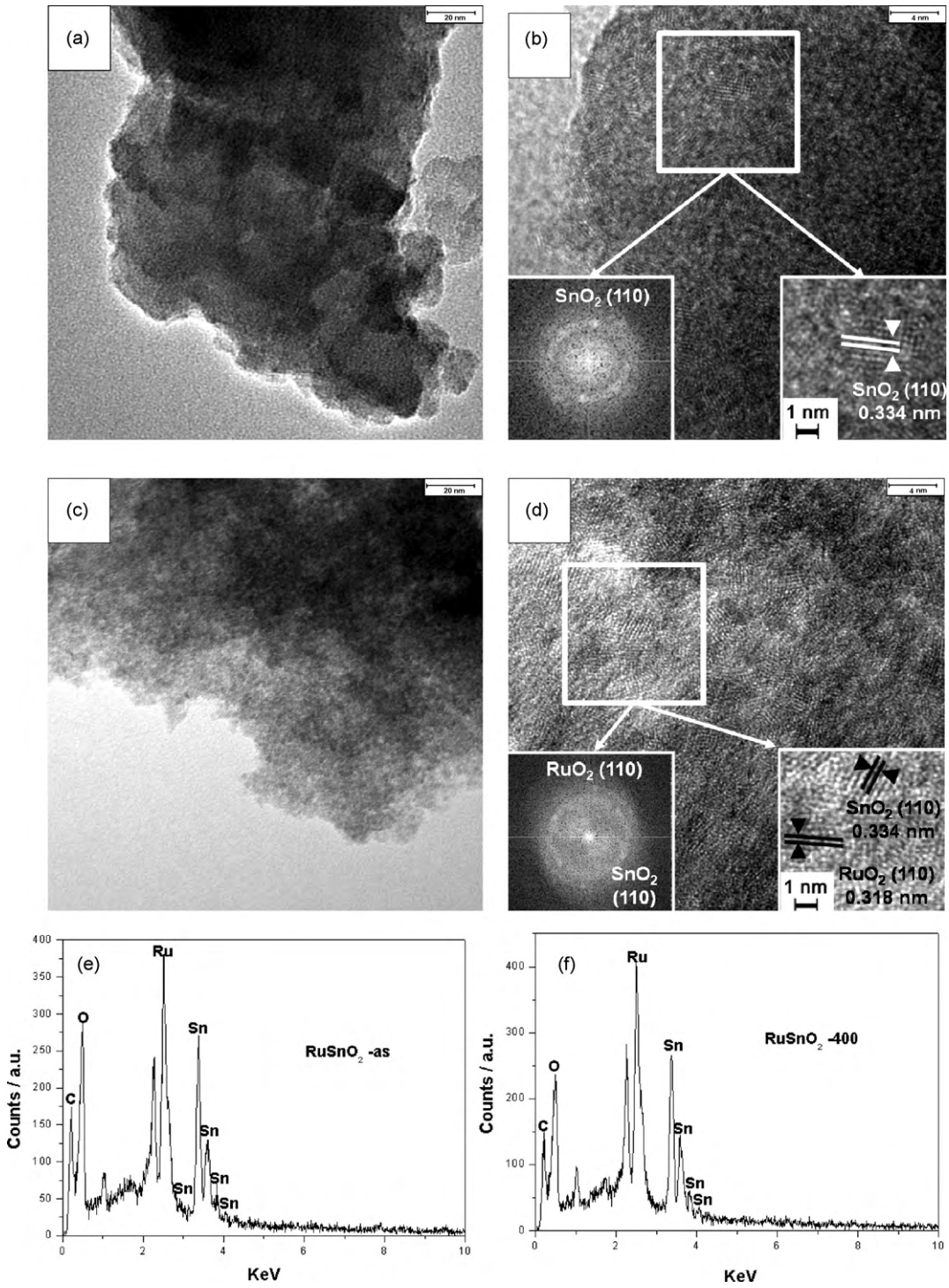

Fig. 2. FE-TEM images and energy dispersive X-ray spectrum of $RuSnO_2$-as (a, b and e) and $RuSnO_2$-400 (c, d and f). The insets of Fig. 2(b) and (d) are selection area diffraction patterns (bottom right) and high-resolution TEM images (bottom left) of the samples, respectively.

For the prevention of reverse reaction, the pH value of the mixture was adjusted by 0.6 M Na_2CO_3 (Aldrich) solution to 5. Then hydrogen peroxide (5 mL) was added to the mixture solution with a flow rate of 1 mL min^{-1}. The pH of the solution must be adjusted to 5 for prevention of reverse reaction. After stirring at room temperature for 1 h, the precipitated powders were repeatedly washed and filtrated with distilled de-ionized water until impurities were completely removed. The powders were dried at 80 °C oven for 6 h. The resulting powder was heated at 400 °C for 2 h in air atmosphere.

To prepare RuO_2–SnO_2 supported Pt (40 wt%) catalysts, the RuO_2–SnO_2 powders (0.1 g) were dispersed into de-ionized water and then $H_2PtCl_6{\cdot}6H_2O$ (Aldrich) was added to the solution and mixed for 1 h. After 1 h, $NaBH_4$ (Aldrich) solution as a reductant with an excess amount was added to the mixture solution with continuous stirring at 25 °C for 2 h. The resulting precipitate was washed with de-ionized water and then was dried at 80 °C oven.

The supports and catalysts were characterized by transmission electron microscopy (TEM) using a Philips CM20T/STEM Electron Microscope system at 200 kV. TEM samples were prepared by placing a drop of the catalyst suspension with ethanol on a carbon-coated copper grid. The elemental composition of the catalysts was investigated by energy dispersive X-ray spectroscopy (EDX, JEOL). Structural analysis of the catalysts was carried out using a Rigaku diffractometer equipped with a Cu K_α radiation source of $\lambda = 0.15418$ nm with a Ni filter. The tube current was 100 mA with a tube voltage of 40 kV. The 2θ between 20° and 80° were explored at a scan rate of 4° min^{-1}. Thermogravimetric analysis (TGA) curves were obtained in a thermal analyzer (SDT Q-600, TA Instruments) in the range of 30–800 °C at a heating rate of 10 °C min^{-1} in air flow of 60 cm^3 min^{-1}.

Electrochemical measurements were carried out using a three electrode cell. A Pt gauze and Ag/AgCl (in saturated KCl) were used as a counter and reference electrode, respectively. The glassy carbon electrode as a working electrode was polished with 1, 0.3, and 0.05 μm Al_2O_3 paste and then washed in de-ionized water. The catalyst ink was prepared by ultrasonically dispersing catalyst powders in an appropriate amount of Millipore water. The electrode was coated onto a glassy carbon working electrode with 4 μL of the catalyst ink. After drying at 50 °C oven, the total loading of catalyst was 50 μg cm^{-2}. The solutions of 0.5 M H_2SO_4 and 2 M CH_3OH + 0.5 M H_2SO_4 were continuously stirred and purged with nitrogen. To identify electrochemical properties and catalytic activity of the catalysts, cyclic voltammograms (CVs) for the catalysts were obtained using a potentiostat (Eco Chemie, AUTOLAB) at room temperature with a scan rate of 50 mV s^{-1}. The current versus time curve for methanol electrooxidation of the catalysts was measured at 0.4 V for 600 s. All potentials are reported with respect to Ag/AgCl.

3. Results and discussion

Fig. 1 shows XRD patterns for as-prepared RuO_2–SnO_2 ($RuSnO_2$-as) and RuO_2–SnO_2 heat treated at 400 °C ($RuSnO_2$-400). To investigate the structure of Sn and Ru oxide phases, as shown in Fig. 1, the XRD patterns of RuO_2–SnO_2 were obtained representing the characteristic peaks of typical SnO_2 structure, that is, (1 1 0) at $2\theta = 26.6°$, (1 0 1) at $2\theta = 33.8°$, (2 0 0) at $2\theta = 37.9°$, (2 1 1) at $2\theta = 51.7°$, and (1 1 2) at $2\theta = 64.7°$. The XRD patterns from the peaks in the $RuSnO_2$-as seem to be mainly associated with tetragonal SnO_2, whereas there seem to be no diffraction peaks of Ru oxides because of an amorphous phase. However, since it is hard to distinguish crystal phases just simply based on the XRD patterns, TEM analysis for the $RuSnO_2$ will be described (Fig. 2). The presence of ruthenium oxide in the $RuSnO_2$-400 is clearly revealed by characteristic diffraction peaks of (1 1 0), (1 0 1), and (2 1 1) planes at $2\theta = 28°$, 35°, and 54.2°, respectively. It is expected that the degree of crystallization increases with heat treatment due to transition of amorphous to crystalline phase, which means that the heat treatment could improve crystallinity of SnO_2 and RuO_2.

The nanostructures of $RuSnO_2$-as and $RuSnO_2$-400 are shown in Fig. 2. The $RuSnO_2$-as displays relatively uniform nanostructures with average crystallite size of ~4 nm, as shown in Fig. 2(a). However, crystalline phases with clear lattice fringes are appeared in the $RuSnO_2$-as (Fig. 2(b)), which the spacing of 0.334 nm in crystalline phases corresponds to the (1 1 0) plane of SnO_2. In contrast, the $RuSnO_2$-400 consists of crystalline structure with average crystallite size of ~5 nm, as shown in Fig. 2(c). In the TEM image of the $RuSnO_2$-400, the d-spacings of 0.334 and 0.318 nm are attributed to the (1 1 0) planes of SnO_2 and RuO_2 (Fig. 2(d)). Accordingly, it is evident that from the TEM analysis, the $RuSnO_2$-as and $RuSnO_2$-400 suggest nanocomposite supports consisting of RuO_2 and SnO_2.

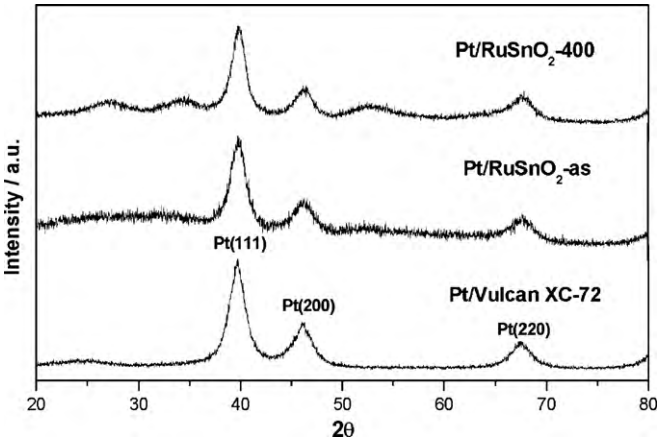

Fig. 3. XRD patterns of $Pt/RuSnO_2$-as, $Pt/RuSnO_2$-400, and Pt/Vulcan XC-72.

The elemental compositions of the nanocomposite electrodes were investigated using an EDX analysis as shown in Fig. 2(e) and (f). The atomic ratio of Ru: Sn in the supports is the nominal composition, which is in good agreement with the intentional one.

Fig. 3 shows XRD patterns of $RuSnO_2$-as and $RuSnO_2$-400 supported Pt (Pt 40 wt%) catalysts ($Pt/RuSnO_2$-as and $Pt/RuSnO_2$-400, respectively) compared to that of Vulcan XC-72 supported Pt catalyst (Pt/Vulcan XC-72). The presence of platinum crystalline structures is clearly revealed by the characteristic diffraction peaks at $2\theta = 39.7°$, 46.2° and 67.4°, which are associated with (1 1 1), (2 0 0) and (2 2 0) planes, respectively. All the XRD patterns clearly show the characteristic peaks of face-centered-cubic structure of Pt crystalline. Fig. 4 shows FE-TEM images of the supported Pt catalysts. The Pt nanoparticles with average crystallite size of ~3 nm are well dispersed and mixed with $RuSnO_2$-as and $RuSnO_2$-400 nanocomposite supports. In the $Pt/RuSnO_2$-as (Fig. 4(a) and (b)) and $Pt/RuSnO_2$-400 (Fig. 4(c) and (d)), the presence of Pt nanoparticles is clearly revealed by lattice fringes with (1 1 1) d-spacing of 0.226 nm. However, the $RuSnO_2$-as consists of crystalline SnO_2 and amorphous RuO_2 while the $RuSnO_2$-400 shows both crystalline SnO_2 and RuO_2. Accordingly, the $RuSnO_2$ supported Pt catalysts are nanocomposite structure consisting of Pt nanocatalysts and SnO_2-RuO_2 nano-supports while Pt catalysts in the Pt/Vulcan XC-72 (Fig. 4(e) and (f)) are deposited on carbon supports (20–50 nm in size).

Fig. 5 shows typical cyclic voltammograms (CVs) of $RuSnO_2$ supported Pt catalysts in 0.5 M H_2SO_4 compared with Pt/Vulcan XC-72. The electrochemical characteristic curves indicate adsorption and desorption region of hydrogen and oxygen as typically observed in polycrystalline platinum electrode. However, the $RuSnO_2$ supported Pt catalysts display thick double layer in the CVs due to oxide species of Ru and Sn compared to Pt/Vulcan XC-72. To characterize catalytic activity toward methanol electrooxidation of the supported Pt catalysts, as shown in Fig. 6(a), CVs were obtained in 2 M CH_3OH + 0.5 M H_2SO_4. The $RuSnO_2$ supported Pt catalysts show higher oxidation current compared with Pt/Vulcan XC-72. This may be primary attributed to oxygen species of RuO_2 and SnO_2 and nanocomposite structure of supports. Especially, it is considered that the nanocomposite structure of RuO_2 and SnO_2 could enhance catalytic activity towards methanol oxidation and reduce the poisoning effect of catalysts from the intermediates [26]. Also, the $Pt/RuSnO_2$-400 shows still higher methanol electrooxidation current than that of the $Pt/RuSnO_2$-as. This means that such an enhanced catalytic activity of the $Pt/RuSnO_2$-400 is attributed to an increased crystallinity of oxide support by means of heat treatment. As shown in Fig. 6(b), chronoamperometry (CA) for the $RuSnO_2$ supported Pt catalysts was measured at 0.4 V in

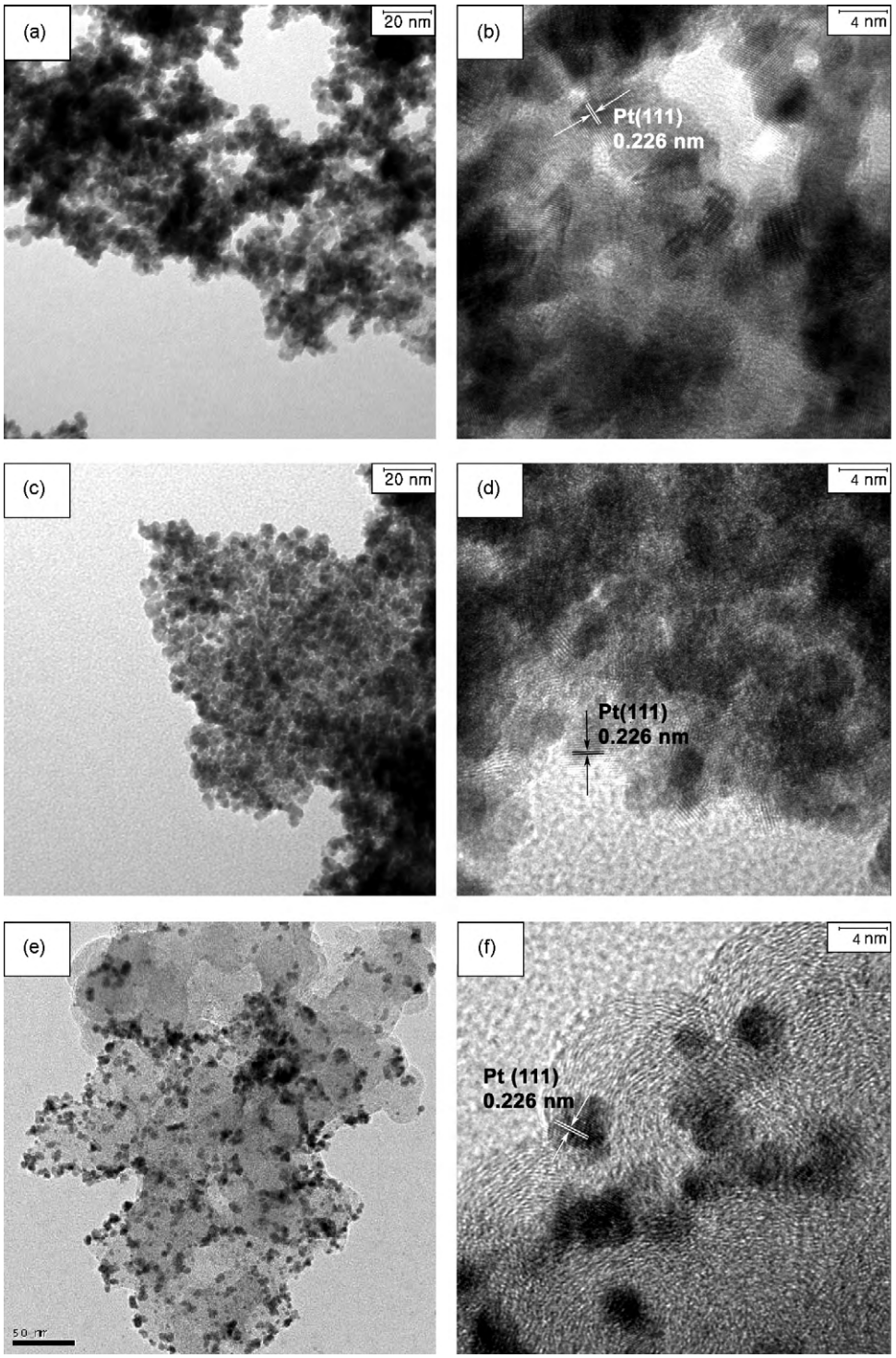

Fig. 4. FE-TEM images of Pt/$RuSnO_2$-as (a and b), Pt/$RuSnO_2$-400 (c and d), and Pt/Vulcan XC-72 (e and f).

2 M CH_3OH + 0.5 M H_2SO_4 compared with Pt/Vulcan XC-72. The sequence of catalytic activity for methanol electrooxidation is as follows: Pt/$RuSnO_2$-400 > Pt/$RuSnO_2$-as > Pt/Vulcan XC-72. The enhanced catalytic activity and stability of the Pt/$RuSnO_2$-400 are due to an increased crystallinity in the nanocomposite support in comparison with the Pt/$RuSnO_2$-as, which might result from improved electrical conductivity of the support as follows: electrical conductivity values of $RuSnO_2$-as and $RuSnO_2$-400 are 6.7×10^{-5} and 3.8×10^{-2} S cm^{-1}, respectively.

Fig. 7 shows thermogravimetric analysis (TGA) curves of supported catalysts in the range of 30–800 °C in air flow. The normalized weight loss of Pt/Vulcan XC-72 is ~80%, which is dominantly attributed to oxidation of the carbon support at around 400 °C. On the other hand, the $RuSnO_2$ supported Pt catalysts show extremely slight weight loss of ~3%, which means an excellent stability of the $RuSnO_2$ supports. Thus, the electrochemical stability of the $RuSnO_2$ supported Pt catalysts could be attributed to corrosion resistance of $RuSnO_2$ compared to Vulcan XC-72.

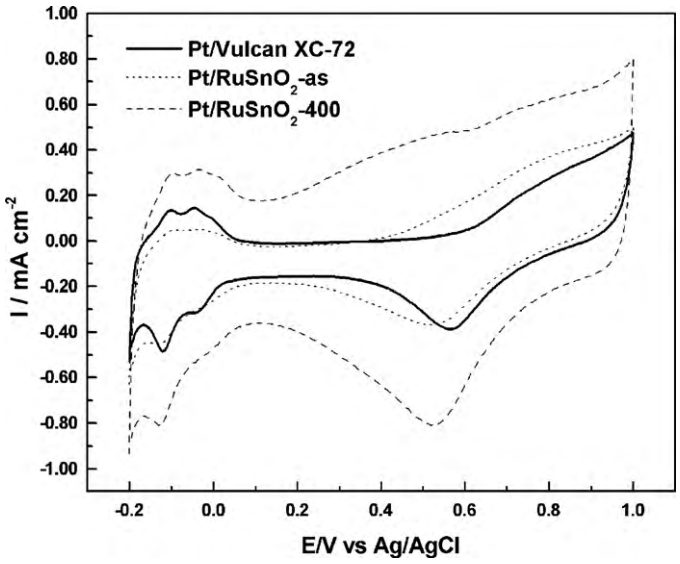

Fig. 5. CVs of supported Pt catalysts in 0.5 M H_2SO_4 with a scan rate of 50 mV s^{-1} at 25 °C.

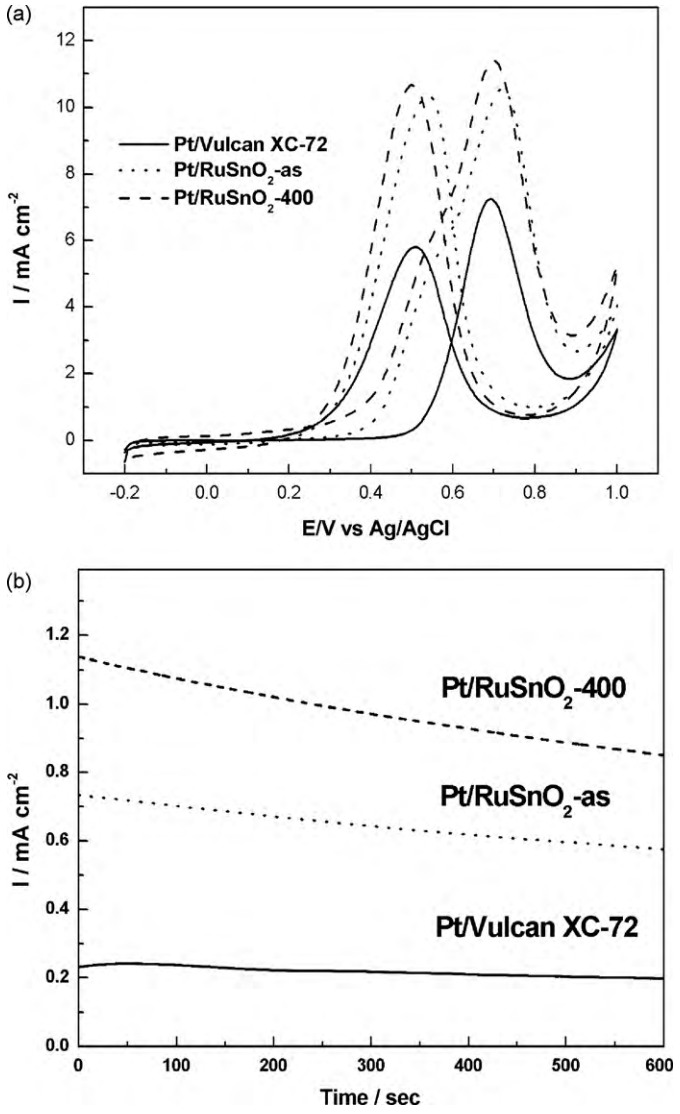

Fig. 6. (a) CVs and (b) plots of oxidation current versus time for supported Pt catalysts in 2 M CH_3OH + 0.5 M H_2SO_4 at 25 °C.

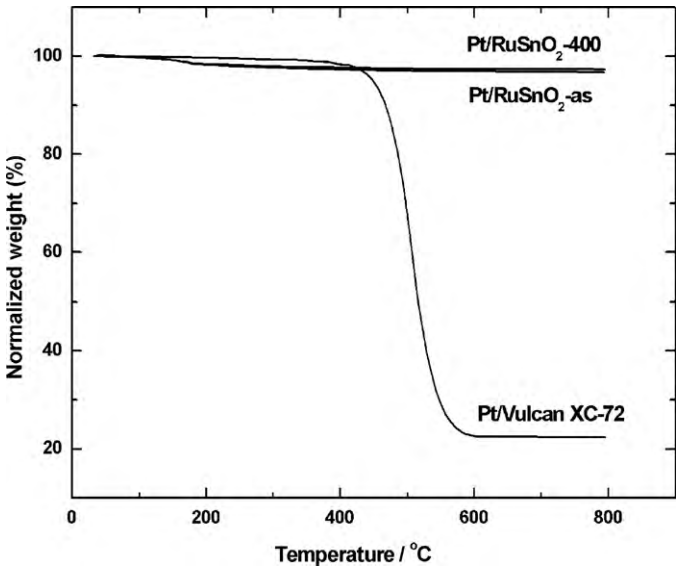

Fig. 7. TGA curves of supported catalysts in the range of 30–800 °C with a heating rate of 10 °C min^{-1} in air flow of 60 SCCM.

4. Conclusions

The RuO_2–SnO_2 nanocomposite supported catalysts for methanol electrooxidation were synthesized. In the case of the $RuSnO_2$ supported catalysts, Pt nanocatalysts with average crystallite size of ~3 nm were well dispersed and mixed with $RuSnO_2$ nanocomposite supports with 4–5 nm in size. The $RuSnO_2$ supported Pt catalysts showed higher oxidation current in comparison with Pt/Vulcan XC-72. Furthermore, the methanol electrooxidation current of the $RuSnO_2$-400 supported Pt catalyst was higher than that of the $RuSnO_2$-as supported Pt catalyst. The improved catalytic activity and catalytic stability of the $RuSnO_2$-400 supported Pt catalyst could be attributed to increased crystallinity and electrical conductivity of oxide support caused by heat treatment and corrosion resistance of $RuSnO_2$.

Acknowledgment

This was supported by a Manpower Development Program for Energy & Resources supported by the Ministry of Knowledge and Economy and the “program for CITG” support program supervised by the NIPA (National IT Industry Promotion Agency) (NIPA-2010-0004).

References

[1] C. Lamy, E.M. Belgsir, J.-M. Leger, J. Appl. Electrochem. 31 (2001) 799–809.
[2] E. Peled, T. Duvdevani, A. Aharon, A. Melman, Electrochem. Solid State Lett. 4 (2001) A38–A41.
[3] S. Maass, F. Finsterwalder, G. Frank, R. Hartmann, C. Merten, J. Power Sources 176 (2008) 444–451.
[4] X. Yu, S. Ye, J. Power Sources 172 (2007) 145–154.
[5] M. Pourbaix, Atlas of Electrochemical Equilibria in Aqueous Solutions, 17, 2nd ed., Nat. Assoc. of Corrosion Engineers, Houston, TX, 1974, p. 1 (Chapter IV).
[6] E. Antolini, J. Mater. Sci. 38 (2003) 2995–3005.
[7] K.H. Kangasniemi, D.A. Condit, T.D. Jarvi, J. Electrochem. Soc. 151 (2004) E125–E132.
[8] D.A. Stevens, J.R. Dahn, Carbon 43 (2005) 179–188.
[9] E. Passalacqua, P.L. Antonucci, M. Vivaldi, A. Patti, V. Antonucci, N. Giordano, K. Kinoshita, Electrochim. Acta 37 (1992) 2725–2730.
[10] M. Wilson, H. Garzon, K. Sickafus, S. Gottesfeld, J. Electrochem. Soc. 140 (1993) 2872–2877.
[11] J. Meyers, R. Darling, 202nd Meeting of the Electrochemical Society, Salt Lake City, 2002 (Abstract 856).
[12] K. Kinoshita, J. Bett, Carbon 12 (1974) 525–533.
[13] H. Binder, A. Kohling, K. Richter, G. Sandstede, Electrochim. Acta 9 (1964) 255–274.

[14] K. Kinoshita, Carbon Electrochemical and Physicochemical Properties, John Wiley & Sons, New York, 1988 (Chapter VI).
[15] X. Wen Lou, Y. Wang, C. Yuan, J.Y. Lee, L.A. Archer, Adv. Mater. 18 (2006) 2325–2329.
[16] E. Antolini, F. Colmati, E.R. Gonzalez, Electrochem. Commun. 9 (2007) 398–404.
[17] F. Delime, J.-M. Leger, C. Lamy, J. Appl. Electrochem. 29 (1999) 1249–1254.
[18] R.J. Brook, in: F.F.Y. Wang (Ed.), Ceramic Fabrication Process, vol. 9, Academic Press, New York, 1976, p. 17 (Chapter 17).
[19] C. Nayral, T.O. Ely, A. Maisonnat, B. Chaudret, P. Fau, L. Lescouzeres, A.P. Lavgne, Adv. Mater. 11 (1999) 61–63.
[20] C.-C. Hu, K.-H. Chang, C.-C. Wang, Electochim. Acta 52 (2007) 4411–4418.
[21] E. Shanthi, V. Dutta, A. Banerjee, K.L. Kopra, J. Appl. Phys. 51 (1980) 6243–6251.
[22] T. Maruyama, K. Tabata, J. Appl. Phys. 68 (1990) 4282–4285.
[23] A.E. Rakhshani, Y. Makdisi, H.A. Ramazaniyan, J. Appl. Phys. 83 (1998) 1049–1057.
[24] K.-S. Lee, I.-S. Park, Y.-H. Cho, D.-S. Jung, N. Jung, H.-Y. Park, Y.-E. Sung, J. Catal. 258 (2008) 143–152.
[25] H.-J. Ahn, H.-C. Choi, K.-W. Park, S.-B. Kim, Y.-E. Sung, J. Phys. Chem. B 108 (2004) 9815–9820.
[26] Z.B. He, J.H. Chen, D.Y. Liu, H.H. Zhou, Y.F. Kuang, Diam. Relat. Mater. 13 (2004) 1764–1770.